Effects of the gravitational field of a neutron star on the emission from hot polar spots on the surface of radio pulsars

Article *in* Astronomy Letters · February 1995

CITATIONS
42

READS
30

3 authors, including:

V. E. Zavlin
Universities Space Research Association
133 PUBLICATIONS **4,085** CITATIONS

SEE PROFILE

Yu. A. Shibanov
Ioffe Institute
150 PUBLICATIONS **1,510** CITATIONS

SEE PROFILE

Astronomy Letters, Vol. 21, No. 2, 1995, pp. 149 - 158. Translated from Pis'ma v Astronomicheskii Zhurnal, Vol. 21, No. 3, 1995, pp. 168 - 178.

Effects of the Gravitational Field of a Neutron Star on the Emission from Hot Polar Spots on the Surface of Radio Pulsars

V. E. Zavlin*, Yu. A. Shibanov, and G. G. Pavlov**, *****

* *St. Petersburg State Technical University, ul. Politekhnicheskaya 29, St. Petersburg, 195251 Russia*

** *Ioffe Physicotechnical Institute, Russian Academy of Sciences, Politekhnicheskaya 26, St. Petersburg, 194021 Russia*

*** *University of Pennsylvania, USA*

Received August 22, 1994

Abstract – Taking into consideration the bending of photon paths in the gravitational field of a neutron star, we investigated the light curves and emission spectra of hot spots at the magnetic poles of a radio pulsar. The atmosphere model for a neutron star with a strong magnetic field is used to describe the radiation arising from the spots. The light curves and spectra differ qualitatively from those obtained under the assumption that the spots emit like a blackbody. The sharp anisotropy of the emergent radiation, in combination with the gravitational effects, gives rise to a significant dependence of the light curves on photon energy (a shift in the phase of the peak, the appearance of an interpulse, and nonmonotonic behavior of the modulation index) and on the mass and radius of the neutron star. Specific calculations were performed for the assumed parameters of PSR 1929+10. Simple analytic expressions were derived for the emission flux from small spots received by a remote observer. The results can be used to interpret the observed thermal emission from isolated pulsars.

INTRODUCTION

X-ray ROSAT observations of thermal emission from a number of radio pulsars [1] open up unique opportunities for experimental study of the thermal evolution of isolated neutron stars. The latter is strongly dependent on the properties of superdense matter in the interior of these stars, about which little is known. Investigation of the cooling of isolated pulsars may provide fundamental physical information on the equation of state of superdense matter, on the presence in it or absence from it of pion or quark condensates, on superfluidity of nucleons, etc. (see, e.g., [2]), which cannot so far be obtained under laboratory conditions.

Such opportunities are offered by high-quality spectra, which allow the effective temperature of the emitting surface of a neutron star to be accurately determined. As a rule, the spectra of thermal emission from the relatively young (with ages in the range $\sim 10^4 - 5 \times 10^5$ years) pulsars Vela [3], PSR 0656+14 [4], PSR 1055-52 [5], and the γ-ray pulsar Geminga [6] consist of two components – soft and hard. The soft component appears to arise from the entire surface of the neutron star. Blackbody fits to its spectrum yield a stellar surface temperature of $\sim 5 \times 10^5 - 2 \times 10^6$ K. The hard component is commonly thought to originate from a hot spot on the polar cap of the neutron star, which is heated by the flow of charged particles produced during operation of the pulsar. Blackbody fits give a spot surface temperature of $\sim (2 - 4) \times 10^6$ K, which is approximately the same for all objects exhibiting a hard component. Both the soft and hard components pulsate with the neutron star's rotation period. The pulsed fraction is ~10 - 50% and varies with photon energy. Pulsations of the hard and soft components are usually shifted in phase. The presence of a hard component alone is a distinctive feature of older pulsars (e.g., PSR 1929+10 and PSR 0950+08). It is suggested that the surface of these objects has cooled down to such an extent that its emission is difficult to observe, while the polar cap remains hot during operation of the radio pulsar.

The spectrum emerging from the surface of a neutron star (in particular, from its small part – a hot spot) may significantly differ from that of a blackbody due to the presence of an atmosphere (see, e.g., [7]). The strong magnetic field of radio pulsars ($B \sim 10^{12} - 10^{13}$ G) makes the atmospheric emission highly anisotropic [8, 9]. The beam acquires the shape of a narrow peak (a pencil) along the magnetic field and a broad maximum (a fan) across the field; the height and width of these peaks depend on the energy of emitted photons and on neutron-star parameters [10]. In previous calculations of the light curves for X-ray emission of hot spots [11, 12], most attention was concentrated on the study of magnetic-field effects, while the effects of light bending in the strong gravitational field of a neutron star were neglected. However, these effects can significantly alter the shape of the light curve of emission originating in the vicinity of the surface of a neutron star (see, e.g., [13, 14]). More specifically, due to warping of space near the star, an observer at infinity can receive emission from the

1063-7737/95/2102-0149$10.00 © 1994 МАИК Наука /Interperiodica Publishing

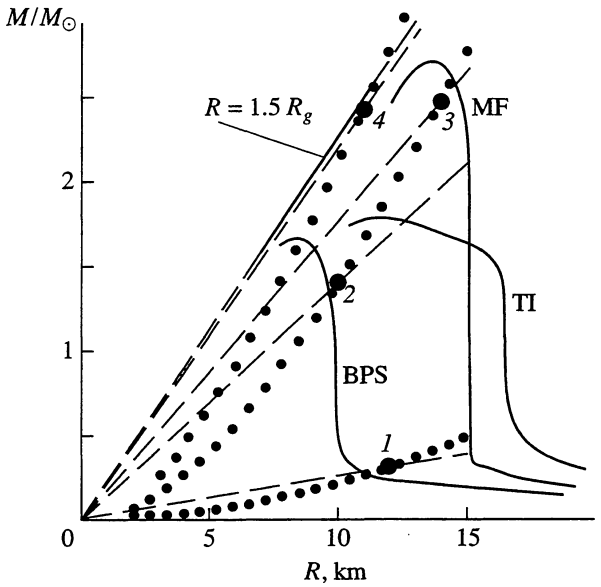

Fig. 1. The range of allowed values of neutron-star masses and radii. The permitted region is bounded by the $M(R)$ relations (solid curves) corresponding to the hardest (MF and TI) and to one of the soft (BPS) equations of state of superdense matter (see, e.g., [20]). The values of M and R for realistic equations of state lie to the right of the $R = 1.5R_g$ straight line. The location of neutron-star models selected for calculations are indicated by circles; the numerals show model numbers according to the table. Dotted and dashed lines represent the lines of constant gravitational acceleration g and parameter g_r.

far stellar hemisphere, which is invisible in flat space. The inclusion of both the gravitational effects and the dependence of the beam on photon energy in a strong magnetic field may result in the appearance of various features in the light curves (variations in shape and magnitude of the pulse with photon energy, a shift in the pulse phase, the appearance of an interpulse at some energies, etc.) observed in the soft X-ray emission of pulsars. If the spots emit like a blackbody, the beam and, therefore, light curves should be independent of the photon energy. Real light curves should also depend on the ratio of the radius of a neutron star to its gravitational radius, i.e., on its mass and radius. The same ratio determines the effect of gravitational redshift in the observed spectrum. Thus, a comparison of theoretical spectra and light curves with observations may place additional restrictions on the mass and radius of the neutron star and, consequently, on the equation of state of matter in its interior.

Parameters of neutron-star models used in calculations

Model	R, km	$M/M_\odot$	g_{14}	g_r	R/R_g	J_{max}, deg
1	11.0	0.264	0.30	0.964	14.15	94.31
2	10.0	1.402	2.43	0.766	2.418	131.8
3	14.0	2.479	2.43	0.691	1.914	159.8
4	11.0	2.425	4.50	0.591	1.538	261.2

In this paper, we calculate the spectra and light curves for the emission originating from hot spots at the magnetic poles of a radio pulsar, with the inclusion of gravitational effects for various values of mass and radius of the neutron star. We use the magnetic-atmosphere model to describe the emission arising from the hot-spot surface. We plot specific curves for the parameters derived from radio and X-ray observations of the pulsar PSR 1929+10. For comparison, we also present the corresponding results for the spots that are assumed to emit like a blackbody. The gravitational effects are allowed for in terms of the Schwarzschild metric, using the approach described in, for example, [14]. This approach, together with simple analytic expressions for estimating the flux from a small spot, are briefly described in the Appendix.

GENERAL DESCRIPTION OF THE MODEL

We assume that the hot spots are formed at the poles of a neutron star, which are heated by relativistic electrons or positrons produced during operation of the pulsar. Because the characteristic depth of energy release for these particles is much greater than the thickness of the spot atmosphere ($\lesssim$1 cm), they have no direct effect on its structure. At the same time, the effective temperature of the atmosphere is determined by the rate of energy release during the deceleration of relativistic particles. For our calculations, we choose the effective temperature $T_{eff} = 2.9 \times 10^6$ K, derived from a preliminary fitting of the observations of PSR 1929+10 by the spectrum of a hydrogen atmosphere [12]. This value was obtained for a magnetic field at the stellar poles of $B = 1.2 \times 10^{12}$ G, which is consistent with the observed properties of the radio pulsar. The selected spot sizes, $R_{sp} = \gamma R = 100$ mm (γ is the spot angular diameter, and R is the stellar radius), correspond approximately to the values predicted by the theory of radio pulsars [15]. The distribution of temperature and magnetic field over the spot area was assumed to be uniform. We take the angles between the rotation axis and the observer's direction and between the rotation axis and the stellar magnetic axis to be $\alpha = 50°$ and $\beta = 30°$ [16], respectively. Various estimates of the distance D to the source are highly uncertain: 30 pc - 2 kpc (see [17]). According to Taylor *et al.* [18], the most plausible value is $D = 170$ pc. For convenience, we normalize the flux to $D = 100$ pc.

To illustrate the dependence of the parameters of emission seen by an observer at infinity on the mass and radius of the neutron star, we select several characteristic points in the mass–radius diagram (see Fig. 1) that are located near the boundaries of the R–M region allowed by various equations of state of stellar matter. On the one hand, these points correspond to various

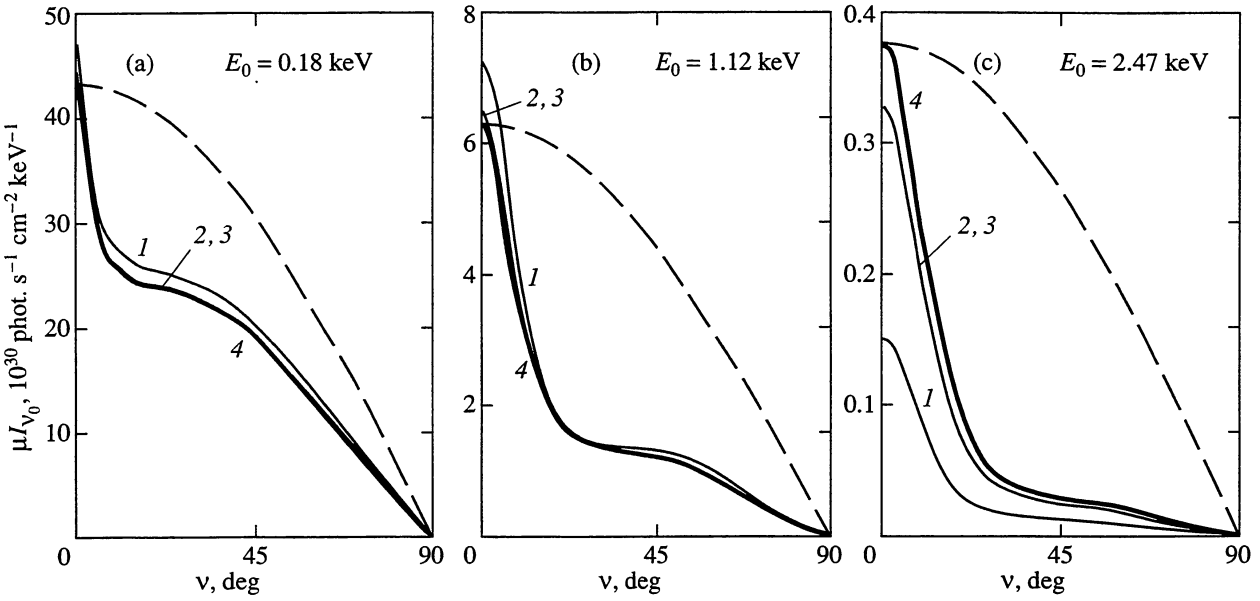

Fig. 2. Angular distributions for the flux emerging from the atmosphere of a hot polar spot on the neutron star (solid lines) for various photon energies E_0. The angular distributions for spots emitting like a blackbody are indicated by dashed lines. The effective temperature and magnetic field at the poles are $T_{\rm eff} = 2.9 \times 10^6$ K and $B = 1.2 \times 10^{12}$ G (see text). The numerals have the same meaning as in Fig. 1.

values of the neutron star's surface gravity,

$$g = \frac{GM}{R^2 g_r} = \frac{1.33 \times 10^2 M}{M_\odot R_{\rm km}^2 g_r} \times 10^{14} = g_{14} \times 10^{14} \text{ cm s}^{-2}, \quad (1)$$

and, consequently, to various parameters of its atmosphere (temperature and density distributions with depth, intensities of the emergent radiation). On the other hand, they correspond to various values of gravitational parameter g_r, which is responsible for the effects of the General Theory of Relativity (GTR),

$$g_r = \sqrt{1 - \frac{2GM}{c^2 R}} = \sqrt{1 - \frac{2.952M}{M_\odot R_{\rm km}}}, \quad (2)$$

where G is the gravitational constant, c is the speed of light, $M_\odot$ is the solar mass, and $R_{\rm km}$ is the stellar radius in km. The parameter g_r is related to the widely used parameter of gravitational redshift z by the formula $g_r = 1/(1+z)$. The values of parameters g_{14}, g_r, M and R, and the ratio of the neutron star's radius to its gravitational radius $R_g = 2GM/c^2$, for four selected points are given in the table. When moving along the dotted lines $g = \text{const}$ in Fig. 1, the properties of emission emerging from the neutron star for the specified values of effective temperature, magnetic field, and atmospheric chemical composition do not change. On the contrary, when moving along the dashed lines, the GTR effects remain unchanged.

Figure 2 shows the angular distributions of the flux from a spot local element on the surface of the neutron star for various energies $E_0 = h\nu_0$ of emitted photons and for various values of parameter g. The magnetic field is directed along the normal to the spot surface, $\mu = \cos\theta$, where θ is the angle between the normal and the wave vector. For comparison, we also present the curves representing the angular distribution of blackbody radiation $I_{\nu_0}(\mu)\mu \propto \mu$; for convenience, they are normalized in such a way that their maximum coincides with the flux peak for model *4*. Notice the emission peak along the magnetic field, whose relative magnitude increases with photon energy and with an increase in g. The origin of the peak is associated with greater atmospheric transparency along the magnetic field [19]. Therefore, we see deeper and hotter layers along the field. The dependence on g results from the fact that atmospheres with large surface gravities are characterized by a steeper temperature rise with depth. At low energies, the atmospheric transparency decreases, the photons emerge from a depth where the temperature gradient is small, and the magnitude of the peak also decreases. The corresponding spectral fluxes are shown in Fig. 3. The spectra of magnetic atmospheres are harder than the blackbody spectrum with the corresponding effective temperature (see, e.g., [9]). The degree of hardness depends on the steepness of the temperature profile and, therefore, on g.

As seen from Figs. 2 and 3, the dependence of the properties of emergent radiation on the position of the star in the R–M plane is rather weak, but it is strong

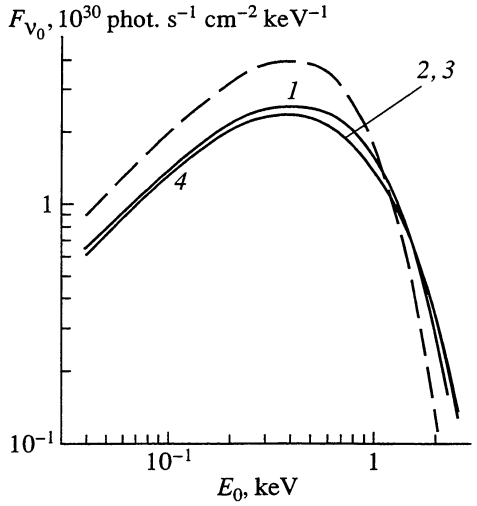

Fig. 3. Spectral fluxes for hot polar spots. Notation and parameters are the same as in Fig. 2.

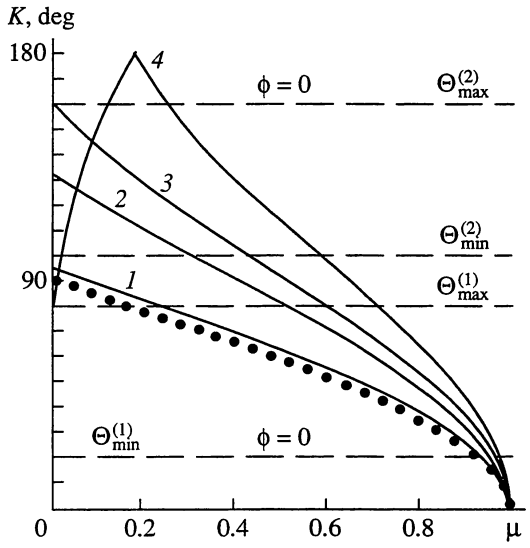

Fig. 4. Polar angle K (measured from the direction of observation) of an emitting point at the neutron-star surface as a function of the cosine of the beaming angle of rays reaching the observer for models *1* - *4* (solid lines). The dotted line represents the $K(\mu)$ relation for the flat-space case ($g_r = 1$). Dashed lines correspond to extreme locations of the centers of two polar spots on PSR 1929+10 at phases $\Phi = 0$ and 0.5.

enough to be taken into account in quantitative calculations. Calculation of the corresponding beaming patterns and spectra is the first step in the subsequent estimation of gravitational effects for emission propagating from the spot to an observer at infinity.

For different neutron-star models from the table, Fig. 4 plots the polar angle K of an emitting point as a function of the cosine of the beaming angle θ for rays emerging from this point and reaching the observer. The angle K is measured from the "star center–observer" axis [see Appendix, expression (A4), for more details]. The horizontal lines correspond to the extreme angular positions $\Theta^{(1,2)}_{min,max}$ of the centers of two hot spots at phases $\Phi = 0$ and 0.5. These phases correspond to the minimum and maximum angular distance from the center of the "main" spot 1 to the observer. $\Theta^{(1)}_{min} = 20°$, $\Theta^{(1)}_{min} = 80°$ and $\Theta^{(2)}_{min} = 100°$, $\Theta^{(2)}_{min} = 160°$ characterize the assumed geometry of the pulsar PSR 1929+10. Figures 2 and 4 give a qualitative insight into the action of gravitational light bending. In flat space ($g_r = 1$), neglecting the small angular diameter of the star, $K = \theta$. Only rays emitted toward the observer by the star's visible hemisphere ($0 \le \mu \le 1$ corresponds to $90° \ge K \ge 0°$) reach the observation point. Figure 4 shows that, in this case, only spot 1 can contribute to the observed flux at all phases. At the same time, the beaming angles of recorded photons vary in the ranges determined by the points of intersection by the corresponding horizontal lines $\Theta^{(1)}_{min}$ and $\Theta^{(1)}_{max}$ of the curve $K(\mu)$ (for $g_r = 1$, we have $20° \le \theta \le 80°$ and $0.175 \le \mu \le 0.94$). The horizontal lines representing spot 2 do not intersect with this curve, so that spot 2 remains out of sight at all phases. It follows from Figs. 2 and 4 that rays emerging from the center ($\theta \simeq 0°$) and the edge ($\theta \simeq 90°$) of the beam never reach the observer. The middle part of its slope is an "operating area". In curved space ($g_r < 1$), the operating area of the beam corresponding to spot 1 narrows and shifts to its peak; the smaller the value of g_r, the larger this shift. Rays propagating in directions that are progressively closer to the normal reach the observer. At the same time, an increasingly larger part of the star's far hemisphere becomes visible. Starting from $g_r \simeq 0.81$, spot 2 becomes visible. Its operating area is initially part of the slope that is adjacent to the edge of the beam. As g_r decreases further, this area broadens and shifts toward the peak. This inevitably leads to a general smoothing of the light curve. Note that, depending on the shape of the beam, a situation is possible at some g_r where the total contribution of both spots at phase 0.5 may be larger than their contribution at phase 0. This results in a 0.5 shift in the phase of the peak of the light curve. For $g_r \simeq 0.657$ ($(R/R_g \simeq 1.76)$, the entire far hemisphere of the star becomes visible. At still smaller values of g_r, some points can be seen many times. In particular, at $g_r = 0.59$, two rays (close to the edge and shifted to the center) emitted at each point of the second spot at different angles θ, i.e., emerging from different portions of the slope of the beam, reach the observer. As seen from Fig. 4, at $g_r = 0.59$, each straight line that lies between $\Theta^{(2)}_{min}$ and $\Theta^{(2)}_{max}$ intersects the curve $K(\mu)$ twice. This may lead to a significant increase in the contribution of the second spot at phase 0. This effect is especially noticeable in the case of an orthogonal rotator (see Appendix and [13] for more details). A similar situation

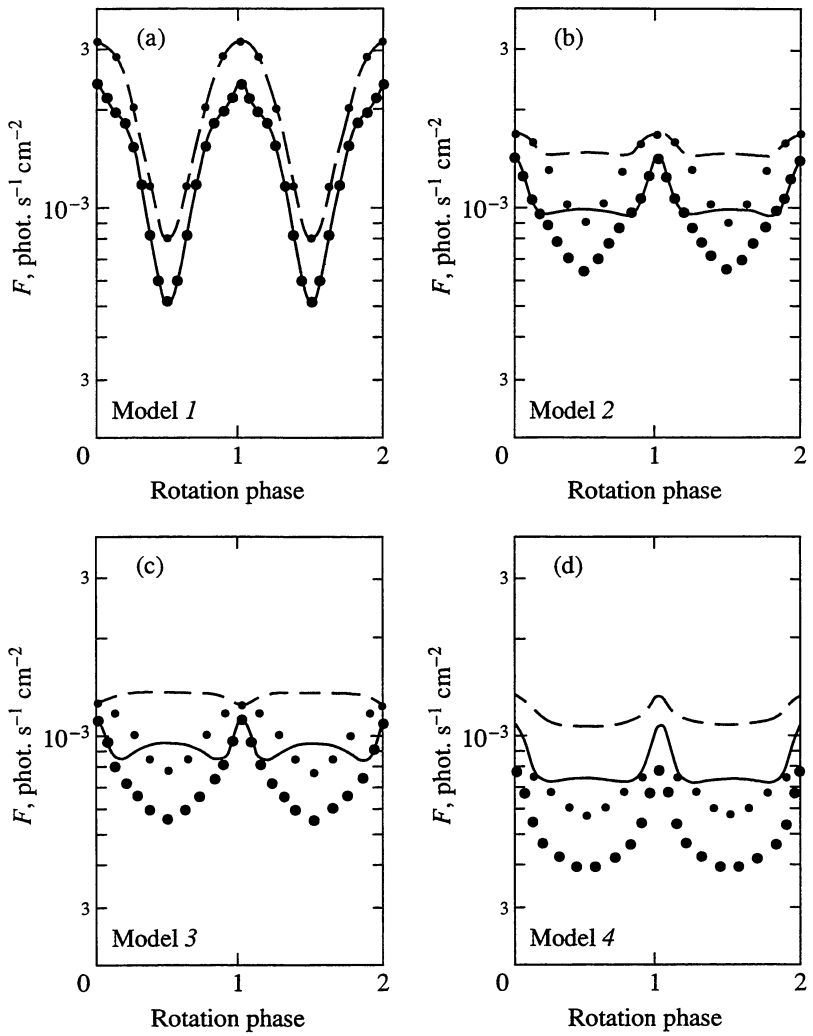

Fig. 5. Bolometric light curves for models *1* - *4* calculated for atmospheric and blackbody radiation of the spots (solid and dashed lines, respectively). Dotted lines indicate the contribution of the main spot.

with an increase in contribution due to a double intersection of the curve $K(\mu)$ is also possible for spot 1, but at still smaller and hardly realistic values of g_r.

Note that the $K(\mu)$ relations are fully determined by the parameter g_r (by the stellar model) and can easily be tabulated. In the Appendix, simple analytic formulas are presented that make it possible to estimate the fluxes from small spots at various rotation phases and for arbitrary parameters and geometry of the pulsar, provided the above relations and the beam of the emergent radiation are known.

RESULTS

Figure 5 plots the energy-integrated light curves calculated for the specified geometry and four selected neutron-star models. We ignore the interstellar extinction. The contribution of the main spot 1, which fully determines the light curve at g_r close to unity (Fig. 5a), is indicated by dotted curves. Clearly, the second spot in the unseen (for $g_r = 1$) stellar hemisphere becomes progressively visible with a decrease in g_r. Its contribution becomes comparable to that of the main spot (Fig. 5b - 5d). In general, this leads to a smoothing of the light curves. Under certain conditions, the phase of the brightness peak may change with a decrease in g_r, when both spots together make a larger contribution at phases close to 0.5 than the main spot at phase 0 (see Fig. 5c, the light curve for a blackbody model). For the model atmosphere and for the same neutron-star parameters, a broad interpulse appears at phase 0.5 (the result of increasing gravitational contribution from the fan part of the beam of the second spot). The figures show that, for not too small values of g_r (in our case, for $g_r \gtrsim 0.6$), the atmospheric light curves qualitatively differ from the blackbody curves:

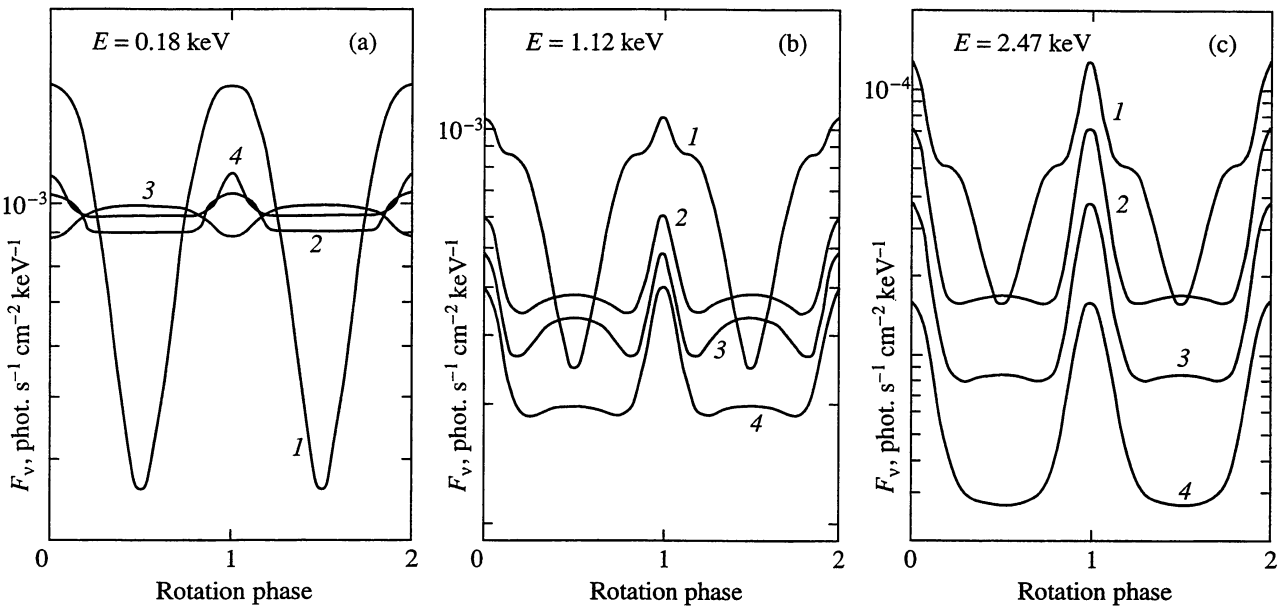

Fig. 6. Light curves for various photon energies E for models *1* - *4*.

the main-pulse shape changes, a broad interpulse appears, the light modulation increases, etc. This results from significant anisotropy of the beam in a strong magnetic field (see Fig. 2). Note also that the peak increases at phase 0 for the smallest value of g_r considered (Fig. 5d), which is associated with a sharp increase in the visible area of the second spot when approaching this phase (see Appendix).

Figure 6 plots the light curves for various photon energies in the frame of an observer at infinity ($E = g_r E_0$). Light curves for the blackbody model are not given, because their shape does not vary with photon energy and coincides with the shape of the corresponding curves in Fig. 5. At low energies (Fig. 6a), when the atmospheric emission is closest to isotropic (see Fig. 2a), the light curves are similar to blackbody ones. At large photon energies (Figs. 6b, 6c), the beam of the emergent radiation changes significantly, and the light curves acquire a characteristic structure that is also observed in the bolometric curves in Fig. 5. For stellar models with g_r close to unity, there is a broad main pulse (a fan) with a sharp peak at the center (the edge of a pencil), which corresponds to the minimum angle between the direction of the magnetic field in the main spot and the observer's direction ($\theta = 20°$) at phase 0. A narrow dip at phase 0.5 results from the main spot approaching the limb of the visible stellar disk. At smaller values of g_r, the main pulse at phase 0 narrows due to gravitational enhancement of the pencil part of the beam from the first spot. At the same time, due to increasing contribution of the fan part of the beam from the second spot, a broad interpulse appears at phase 0.5, which is gradually smeared as g_r decreases further. At certain values of g_r, the phase of the brightness peak may change its position with an increase in energy (see curves *3* for $g_r = 0.69$ in Fig. 6). In our model, this effect results from the combined influence of the gravitational and magnetic fields. The presence of this effect on real light curves, in principle, makes it possible to determine the parameter g_r and, therefore, to constrain the position of the neutron star in the R–M plane, provided the orientation of the magnetic and rotation axes are known.

The degree of modulation $m = (F_{\nu,\max} - F_{\nu,\min})/(F_{\nu,\max} + F_{\nu,\min})$, on average, increases with photon energy from ~10 - 60% to ~70 - 90%.

Figure 8 plots phase-averaged emission spectra. The spectra at different phases of the light curve are more informative; however, their analysis during data reduction is, as a rule, hampered by insufficient photon statistics. Evidently, the observed magnetic spectra are harder than the corresponding blackbody spectra (compare with Fig. 3). The relative positions of the spectra for models *1* - *4* in Fig. 8 are opposite to their relative positions in Fig. 3, which is largely explained by different gravitational redshifts. Because the beam shape of the emergent radiation depends on photon energy, the bending of photon paths also affects the shape of the spectra. Therefore, the relative positions of the atmospheric spectra differ slightly from those of blackbody spectra.

DISCUSSION

Our results show that the strong magnetic field and the presence of an atmosphere in hot spots on neutron stars qualitatively affect the light curves and spectra of observed thermal emission, as compared to the model

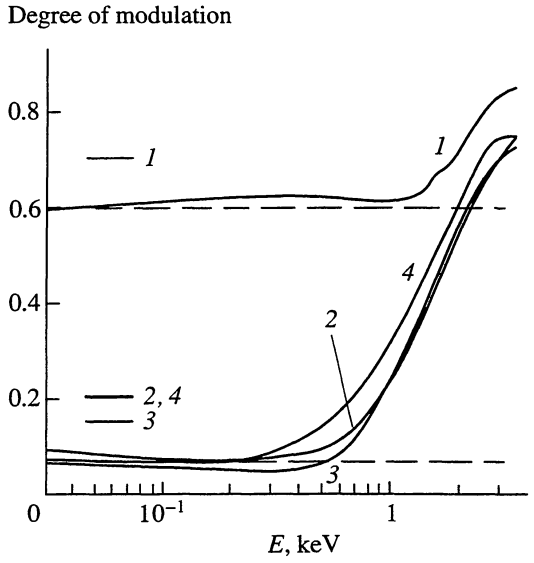

Fig. 7. Dependence of the degree of modulation $m = (F_{\nu,\max} - F_{\nu,\min})/(F_{\nu,\max} + F_{\nu,\min})$ on photon energy for atmospheric and blackbody spot emission (solid and dashed lines, respectively). The horizontal bars on the left indicate the degree of modulation for the bolometric light curves in Fig. 5. Model numbers are denoted by numerals.

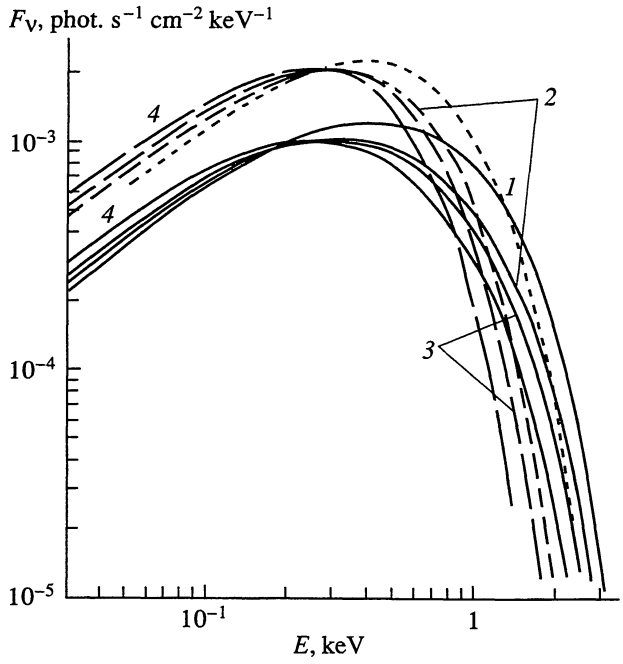

Fig. 8. Phase-averaged spectral fluxes. Notation is the same as in Fig. 7.

of blackbody radiation commonly used in data reduction. They indicate that magnetic-atmosphere radiation is much more sensitive to the effects of a stellar gravitational field due to the presence of a highly anisotropic beam and its dependence on photon energy. This provides additional possibilities for obtaining information from observations not only about polar-spot parameters (particularly about the location of the magnetic poles on the surface and their orientation relative to the rotation axis) but also about the mass and radius of the neutron star and, therefore, about its internal structure.

We selected pulsar PSR 1929+10 as an illustration. Comparison of the theory with observations requires the inclusion of interstellar extinction and the convolution of data with the detector response matrix, which is beyond the scope of this paper. Nevertheless, as follows from our results, the interpretation of observations of this pulsar in terms of the above magnetic-atmosphere model must significantly affect the estimates of its parameters obtained by Yancopoulos *et al.* [17], who assumed that the spots emit like a blackbody. Preliminary results show that the application of magnetic-atmosphere spectra eliminates two main conflicts with the theory of radio-pulsar hot polar caps that follow from blackbody interpretation – excessively high temperature $\simeq 4 \times 10^6$ K and excessively small spot diameters $\simeq 30(D/250$ pc) m. Application of the magnetic-atmosphere model gives a temperature one and a half times lower and spot diameters three times larger, which makes them consistent with theoretical predictions [15].

Because the magnetic-atmosphere emission is much more anisotropic than blackbody radiation, the observed modulation (~20 - 40%) does not require large values of $R/R_g(\simeq 3.9)$ that follow from blackbody interpretation [17]. For example, the light curves near the maximum of the spectrum (see Fig. 6b) preserve a ~ 30% degree of modulation even for model *4* (g_r = 0.59, R/R_g = 1.53; R = 5.9 km for M = 1.3 $M_\odot$, instead of 15 km for blackbody interpretation). It should be emphasized that the shape of the calculated light curves for small values of g_r differ significantly from a sine wave, whereas Yancopoulos *et al.* [17] conclude that the observed light curve can be approximated by a sinusoidal law. It should be kept in mind, however, that the number of photons ($\simeq$420) recorded from PSR 1929+10 by the ROSAT observatory is too small to enable us draw reliable conclusions about the shape of the light curve. It is hoped that future observations of this and similar sources (particularly from the ASCA satellite), interpreted in terms of the magnetic- atmosphere model, will enable the properties of the emitting region and neutron-star parameters to be determined to a higher accuracy.

ACKNOWLEDGMENTS

This study was partially financed by the Russian Foundation for Fundamental Research, project no. 93-02-2916;

ESO C & EE, grant no. A-01-068; and ISF, grant no. R6A000. The work of G.G. Pavlov was supported by NASA, grant no. NAGW-1522.

APPENDIX

Let a hot spot with a small angular diameter ($\gamma \ll 1$) lie at the magnetic pole of a star with a dipolar magnetic field. We assume that the magnetic field within such a small spot is constant in magnitude and is in the direction of the normal to the surface of the star of radius R at each point of the spot. In this case, the intensity emitted by each element of the spot is an axisymmetric function $I_{\nu_0}(\mu)$, where μ is the cosine of the angle θ between the normal and wave vector and ν_0 is the emission frequency in the frame of the neutron star. Following Riffert and Meszaros's paper [14], we write the expression for the flux at frequency $\nu = g_r\nu_0$, as seen by an observer at a distance D from the star, as

$$F_\nu(\Theta, D) = 2\left(\frac{R}{D}\right)^2 g_r \int \phi_L I_{\nu_0}(\mu)\mu d\mu, \qquad \text{(A1)}$$

where Θ is the polar angle of the spot center in a coordinate system with the Z axis directed from the stellar center to the observer and $2\phi_L = 2\phi_L(\gamma, \Theta, \mu)$ is the length of the azimuthal arc of the emitting region in the same coordinate system for fixed values of μ. The expression for ϕ_L has the form

$$\phi_L = \begin{cases} \cos^{-1}(B), & -1 \le B \le 1, \\ 0, & B > 1, \\ \pi, & B < -1, \end{cases} \qquad \text{(A2)}$$

$$B = \frac{\cos\gamma - \cos(K - \Theta)}{\sin\Theta \sin K} + 1, \qquad \text{(A3)}$$

where $K = K(\mu)$ is the angle between the direction of observation and the radius vector from the stellar center to a point from which the emission is beamed at an angle θ to the observer:

$$K = \begin{cases} J - 2\pi n, & 2\pi n \le J \le \pi(2n+1), \\ 2\pi(n+1) - J, & \pi(2n+1) < J \le 2\pi(n+1), \end{cases} \qquad \text{(A4)}$$

$$J = \frac{b}{R_g}\int_0^{\frac{R_g}{R}} dx \left[1 - (1-2x)\,x^2\left(\frac{b}{R_g}\right)^2\right]^{-\frac{1}{2}}, \qquad \text{(A5)}$$

where n is the integral part of the ratio J/π, $b = (R/g_r)(1-\mu^2)^{1/2}$ is the apparent impact parameter for a ray with the beam angle θ, and $R_g = 2GM/c^2$ is the gravitational radius. The values of $J_{\max} = J(\mu = 0)$ for the neutron-star models used in our calculations are given in the table. The limits of integration over μ can be derived from relations (A2) - (A5).

If the intensities I_{ν_0} are known, then formulas (A1) - (A5) are sufficient for calculating the observed flux from a hot spot with a given orientation Θ and angular diameter γ. Θ is related to the angles between the pulsar's rotation axis and the observer direction α and between the magnetic field and the rotation axis β and to the star's rotation phase Φ by the expression

$$\cos\Theta = \cos\alpha\cos\beta + \sin\alpha\sin\beta\cos(2\pi\Phi). \qquad \text{(A6)}$$

Below, we derive simple analytic expressions that give an accurate result for F_ν for arbitrary orientation of the small spot and make it possible to estimate the flux as a function of source parameters and angular distribution of the emergent radiation.

For a small spot, we may factor the intensity outside the integral sign in expression (A1) and write the flux in the form

$$F_\nu = \frac{S_a}{D^2} g_r^3 I_{\nu_0}(\bar{\mu}), \qquad \text{(A7)}$$

$$\int F_\nu d\nu = \frac{S_a}{D^2} g_r^4 \int I_{\nu_0}(\bar{\mu}) d\nu_0, \qquad \text{(A8)}$$

where $\bar{\mu} = \mu(K = \Theta)$, and

$$S_a = \frac{2R^2}{g_r^2}\int \phi_L \mu d\mu \qquad \text{(A9)}$$

is the apparent spot area.

For a small spot located near the center of the visible disk ($\Theta \ll \gamma$), it follows from (A2) and for $K \le \gamma$ that $B < -1$ and $\phi_L = \pi$. From (A4) and (A5), we obtain $K \simeq \sin\theta/g_r \simeq \theta/g_r$. Then,

$$\int \mu d\mu = \frac{g_r^2\gamma^2}{2}, \qquad \text{(A10)}$$

and

$$S_a = \pi R^2 \gamma^2 \bar{\mu}, \qquad \text{(A11)}$$

where $\bar{\mu} \simeq 1$.

We now assume that the spot is displaced from the "stellar center–observer" axis by a distance that is much larger than its diameter, $\sin\Theta \gg \gamma$. Denote $\Theta - K$ by Δ. We then have

$$\cos\phi_L = B \simeq 1 + \frac{\Delta^2 - \gamma^2}{2\sin^2\Theta}, \qquad \phi_L \simeq \frac{\sqrt{\gamma^2 - \Delta^2}}{\sin\Theta}, \quad -\gamma \le \Delta \le \gamma, \qquad \text{(A12)}$$

and

$$S_a = \frac{2R^2}{g_r^2}\int \sqrt{\gamma^2 - \Delta^2}\,\frac{d\mu}{\sin\Theta}. \qquad \text{(A13)}$$

Since $d\mu = \sin K[d\mu/d(\cos K)]d\Delta$, $\sin K \simeq \sin\Theta$, and the derivative $d\mu/d(\cos K)$ is a smooth function of Δ, the flux is proportional to

$$\int_0^\gamma d\Delta\sqrt{\gamma^2 - \Delta^2} = \frac{\pi\gamma^2}{4}, \qquad \text{(A14)}$$

that is,

$$S_a = \pi R^2\gamma^2\bar{\mu}\frac{1}{g_r^2\sin\Theta}\left|\frac{d\mu}{dK}\right|_{K=\Theta}. \qquad \text{(A15)}$$

By means of (A4) and (A5), it can be shown that $(g_r^2\sin K)^{-1}|d\mu/dK| \simeq 1$ for $K \leq \pi/2$ and that for $\Theta \leq \pi/2$ the area S_a is given by the same expression (A11) as for small values of Θ. In the general case, S_a is fully determined by the $K(\mu)$ dependence, which can be tabulated for various values of g_r.

Figure 9 shows the behavior of factor $(\mu/\sin K)|d\mu/dK|$ for the set of g_r values used in our calculations. For $g_r \geq 0.7$, this factor is, to a high accuracy, equal to μg_r^2 for all values of μ, i.e., S_a is also described by expression (A11). If $g_r < 0.657$, when $J(\mu = 0) > \pi$, then, for $\mu = \mu_*$ corresponding to $K = \pi$, the singularity $\propto(\sin K)^{-1}$ exists in the dependence of this factor on μ. Formula (A15) is applicable if we are not too close to μ_*: $|\pi - \Theta| \sim \sin K \gg \gamma$. As Θ approaches π–γ, the apparent area increases, which leads, for example, to an increase in the main maximum of the light curve in Fig. 5d.

Note that, in the range where expression (A15) is applicable, the apparent radius of the spot coincides with its true radius, $R_a = R_{sp} = \gamma R$, whereas the apparent radius of the image of the entire star is $1/g_r$ times larger than the true radius, $R_a = R/g_r$.

For $|\Theta - \pi| \ll \gamma$ and $g_r < 0.657$, we have $\phi_L = \pi$ for $\pi - \gamma < J < \pi + \gamma$ and $\phi_L = 0$ outside this range. The apparent area is

$$S_a = \frac{2\pi R^2}{g_r^2}\int\mu d\mu \simeq \frac{2\pi R^2\bar{\mu}}{g_r^2}\Delta\mu \simeq \frac{2\pi R^2\gamma}{g_r^2}\bar{\mu}\left|\frac{d\mu}{dK}\right|_{K=\pi}, \qquad \text{(A16)}$$

where $\bar{\mu} = \mu_*$.

As would be expected, (A15) and (A16) are joined at $\Theta \simeq \pi - \gamma$. The increase in S_a as $\Theta \longrightarrow \pi$ is associated with the fact that the spot image turns into a ring. The ring center lies at the center of the disk (stellar image); the central circumference of the ring has the radius $(R/g_r)\sqrt{1-\mu_*^2}$, and its thickness is $\simeq(R\gamma/g_r)\mu_*|d\mu/dK|(1-\mu_*^2)^{-1/2}$. If the spot center is slightly displaced from the point $\Theta = \pi$, its image splits: the ring is broken down into two crescents with different radii and different extent. For $g_r < 0.581$, the center of the stellar hemisphere facing the observer also becomes visible twice – at $\mu = 1$ and $\mu = \mu_{**}$, where $J(\mu_{**}) = 2\pi$. As a result, the image of the corresponding spot consists of a circle with area (A11) and a ring whose area is given by expression (A16) for $\bar{\mu} = \mu_{**}$ and for the derivative $d\mu/dK$ taken at $J = 2\pi$. At still smaller values of g_r, multiple images of the stellar surface are formed.

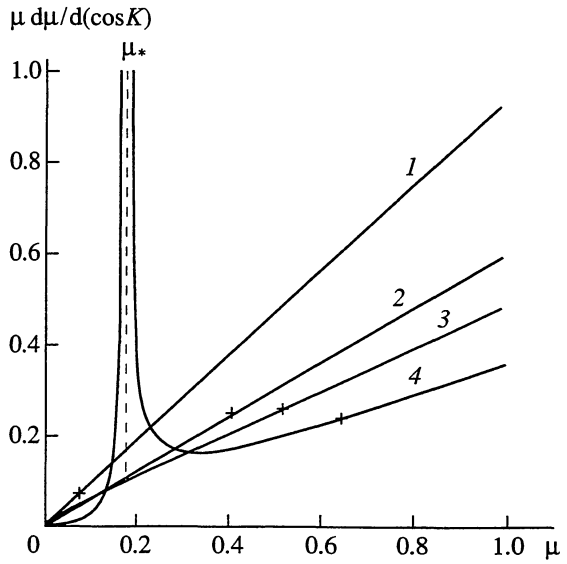

Fig. 9. The factor characterizing the apparent surface area of a small spot versus the cosine of the beaming angle of photons [see expression (A15)] for models *1* - *4* (numerals beside the curves). The crosses correspond to $K = \pi/2$; expression (A11) is applicable to the right of the crosses. The value $\mu = \mu_*$ (which exists for model *4* only) is determined by the condition $K(\mu_*) = \pi$.

Note that the above formulas are valid for $g_r > 1/\sqrt{3} \simeq 0.577$ ($R/R_g > 1.5$). This condition is satisfied for all known equations of state of a neutron star.

REFERENCES

1. Ögelman, H., *Lives of Neutron Stars*, Alpar, A., *et al.*, Eds., Dordrecht: Kluwer, 1994 (in press).
2. Pethick, C.J., *Rev. Mod. Phys.*, 1992, vol. 64, p. 1133.
3. Ögelman, H., Finley, J.P., and Zimmerman, H.U., *Nature*, 1993, vol. 361, p. 136.
4. Finley, J.P., Ögelman, H., and Kiziloğlu, Ü., *Astrophys. J. Lett.*, 1992, vol. 394, p. L19.
5. Ögelman, H. and Finley, J.P., *Astrophys. J. Lett.*, 1993, vol. 413, p. L31.
6. Halpern, J.P. and Ruderman, H., *Astrophys. J.*, 1993, vol. 415, p. 286.
7. Romani, R.W., *Astrophys. J.*, 1987, vol. 313, p. 718.

8. Shibanov, Yu.A., Zavlin, V.E., Pavlov, G.G., and Ventura, J., *Astron. Astrophys.*, 1992, vol. 266, p. 313.
9. Pavlov, G.G., Shibanov, Yu.A., Zavlin, V.E., and Meyer, R., *Lives of Neutron Stars*, Alper, A., *et al.*, Eds., Dordrecht: Kluwer, 1994 (in press).
10. Shibanov, Yu.A. and Zavlin, V.E., *Astron. Lett.*, 1995, vol. 21 (in press).
11. Shibanov, Yu.A., Zavlin, V.E., Pavlov, G.G., and Ventura, J., Lives of Neutron Stars, Alper, A., *et al.*, Eds., Dordrecht: Kluwer, 1994 (in press).
12. Pavlov, G.G., Shibanov, Yu.A., Ventura, J., and Zavlin, V.E., *Astron. Astrophys.*, 1994 (in press).
13. Pechenick, K.R., Ftaclas, C., and Cohen, J.M., *Astrophys. J.*, 1983, vol. 274, p. 846.
14. Riffert, Y. and Mészáros, P., *Astrophys. J.*, 1988, vol. 325, p. 207.
15. Arons, J., *Astrophys. J.*, 1981, vol. 248, p. 1099.
16. Phillips, J.A., *Astrophys. J. Lett.*, 1990, vol. 361, p. L57.
17. Yancopoulos, S., Hamilton, T.T., and Helfand, D., *Astrophys. J.*, 1994 (in press).
18. Taylor, J.H., Manchester, R.N., and Lyne, A.G., *Astrophys. J.*, 1994 (in press).
19. Kaminker, A.D., Pavlov, G.G., and Shibanov, Yu.A., *Astrophys. Space Sci.*, 1982, vol. 86, p. 249.
20. Shapiro, S. and Teukolsky, S., *Black Holes, White Dwarfs, and Neutron Stars*, New York: Wiley, 1983.